A Subsonic, High-Angle-of-Attack Flow Investigation at Several Reynolds Numbers

Mark H. Clarkson*
University of Florida, Gainesville, Fla.
and
Gerald N. Malcolm† and Gary T. Chapman‡
NASA Ames Research Center, Moffett Field, Calif.

Tests conducted in the Ames 12-Ft Pressure Wind Tunnel on a rotating research body at angles of attack of 45-90 deg yielded results that were inconsistent with simple crossflow theory. Consequently, force and pressure distribution tests, along with oil and sublimation flow visualization studies, were conducted in the same tunnel on a nonrotating model in an attempt to explain the behavior observed in the rotary tests. These studies indicate that, at appropriate conditions of Reynolds number and angle of attack, inflexional instabilities occur in the boundary layer which materially affect separation and, hence, the aerodynamic forces. Calculations of crossflow Reynolds numbers are made and compared with other works on inflexional instability.

Nomenclature

A = body reference area, $\pi d^2/4$
C_p = pressure coefficient, $(p_s - p)/q$
C_{pn} = pressure coefficient based on component of flow normal to axis of body, $C_p/\sin^2\sigma$
C_y = body side force/qA
C_z = body normal force/qA
d = diameter of centerbody, 0.0762 m (0.25 ft)
M = freestream Mach number
p_s = local static pressure
p = freestream static pressure
q = freestream dynamic pressure
R_c = crossflow Reynolds number, $3\delta^* |V_c|_{max}/\nu$
R_d = Reynolds number = $V_t d/\nu$
R_n = $U_\infty d/\nu$
U_∞ = $V_t \sin\sigma$
V_∞ = $V_t \cos\sigma$
V_c = crossflow velocity in boundary layer (Fig. 11)
V_t = magnitude of freestream velocity vector
x = arc length measured from flow dividing line
x_l = arc length measured from station zero on lee side (Fig. 2)
x_w = arc length measured from station zero on windward side (Fig. 2)
δ^* = boundary-layer displacement thickness
ν = kinematic viscosity
σ = angle between the freestream velocity vector and the body longitudinal axis
ψ = angle of roll about the body x axis

I. Introduction

THE study of high-angle-of-attack aerodynamics has received increased attention and support with the objective of providing information for the design of well-controlled, highly maneuverable aircraft. A substantial program, carried on at the Ames Research Center since 1973, emphasizes the determination of aerodynamic coefficients on bodies undergoing rotation or spin. In June 1974, an existing small-scale rotary apparatus, originally built for the Ames 6-×6-Ft Wind Tunnel for testing bodies of revolution, was modified for exploratory tests with an airplanelike model in the Ames 12-Ft Pressure Wind Tunnel.[1] As would be expected from simple crossflow theory[2] (reviewed in Sec. IV.B), these tests showed a strong dependence of the aerodynamic forces and moments on Reynolds number at angles of attack of 75 and 90 deg for the selected body having a square cross section with rounded corners.

The behavior of the spinning moment coefficient with Reynolds number at angles of attack of 45 and 60 deg, although anticipated to some extent, could not be explained on the basis of simple crossflow theory. Furthermore, some of the data obtained in the lower Reynolds number range were suspect because of the low sensitivity of the balances used in the force measurements.

Therefore, a second series of tests, using specially built balances to increase the sensitivity to side force, was carried out in the 12-ft wind tunnel in the summer of 1975. These tests were divided, for convenience, into rotary and nonrotary categories. The data from the rotary portion of that test, as well as a description of a new rotary apparatus, were reported in Ref. 3. In addition, it was shown that the major features of rotary data could be deduced from side-force data taken under nonrotary conditions for the body being investigated. To obtain further insight into the flow behavior and, in particular, to investigate the reasons for the failure of simple crossflow theory to predict the behavior at $\sigma = 45$ and 60 deg, pressure distribution measurements and oil flow and sublimation visualization studies were made with a nonrotating model. This paper analyzes the data from the tests with nonrotating models to determine the flow phenomena that lead to these large changes in side force and, hence, spin moments with changes in Reynolds number and angles of attack.

II. Description of Experiments

A. Test Facility and Test Conditions

The Ames 12-Ft Pressure Wind Tunnel is a variable-pressure, low-turbulence facility with a Mach number range of 0.1 to 0.98 and a maximum unit Reynolds number

Presented as Paper 77-180 at the AIAA 15th Aerospace Sciences Meeting, Los Angeles, Calif., Jan. 24-26, 1977; submitted April 5, 1977; revision received Aug. 1, 1977.

Index categories: Aerodynamics; Boundary-Layer Stability and Transition; Subsonic Flow.

*Professor, Department of Engineering Sciences. Associate Fellow AIAA.
†Acting Assistant Chief, Aerodynamic Research Branch. Member AIAA.
‡Chief, Aerodynamic Research Branch. Member AIAA.

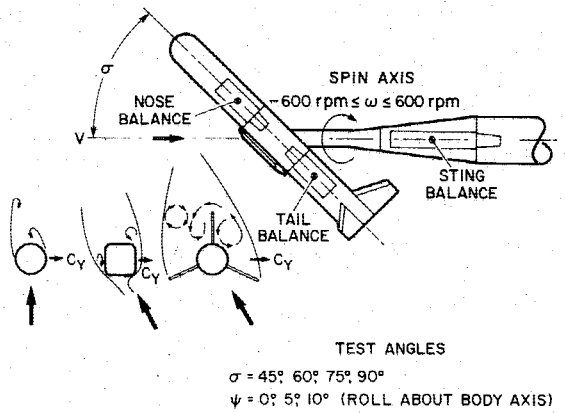

Fig. 1 Model and balance combinations and some prospin flow mechanisms.

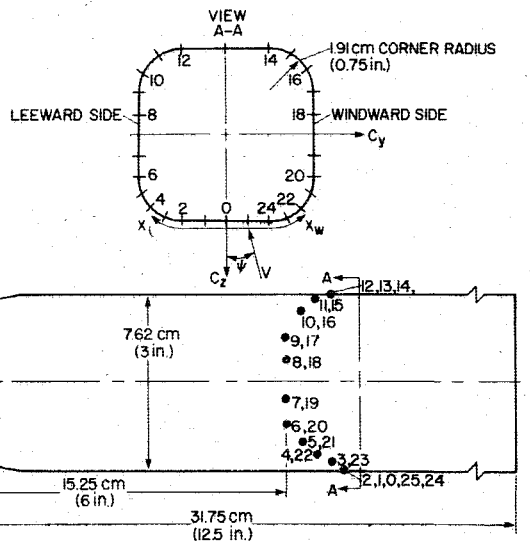

Fig. 2 Location of pressure taps on pressure model.

capability of 29.5×10^6 m^{-1} (9×10^6 ft^{-1}) at $M = 0.25$. Most of the tests were conducted at $M = 0.25$, although a few runs were made at $M = 0.1$ for comparison. The Reynolds number was varied from a maximum of 1.5×10^6 based on a model cross-sectional width of 7.62 cm (3.0 in.) to a minimum of 0.1×10^6. The sublimation tests, to be described later, were run at atmospheric pressure corresponding to $R_d = 0.4 \times 10^6$.

B. Models

Figure 1 is a sketch of some of the prospin flow mechanisms previously investigated[1]; included are asymmetric vortices on a tangent ogive nose, asymmetric flow on a square-cross-section forebody with a hemispherical-shaped nose, and vortex flow over a simple tail configuration. The model nose with a square cross section also was used for the static nonrotating force data presented here, as well as for the oil flow and sublimation studies. Another model with the same shape was used for the pressure distribution tests. This model contained 26 pressure taps, as shown in Fig. 2. The orifices were located at different axial stations to simplify their installation. The small variation in axial location is believed to be acceptable for reasons given in Sec. IVA. Table 1 shows the location of the pressure taps in terms of arc length measured along the surface from point 0 as shown in Fig. 2. The majority of the static tests were conducted with the nose rolled about its longitudinal axis to $\psi = 10$ deg. The geometry of the nose section was selected for study because this cross section is known to be sensitive to Reynolds number, as demonstrated by the rather extensive two-dimensional, static aerodynamic data on this cross section obtained by Polhamus.[4,5]

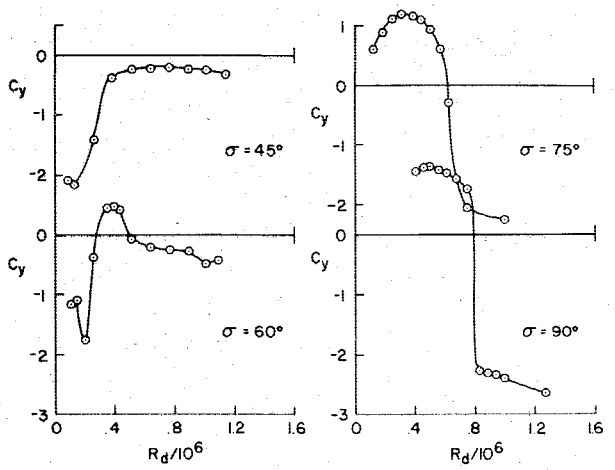

Fig. 3 Effect of Reynolds number at $M = 0.25$ on static side force for $\sigma = 45$, 60, 75, and 90 deg, and $\psi = 10$ deg.

C. Flow Visualization Studies

The surface oil flow studies utilized a mixture of black oxide pigment and lubricating oil, with a few drops of oleic acid added to prevent coagulation of the pigment. This mixture was smeared on the surface of the force model by hand. As the test Reynolds number was increased, an increase in viscosity of the oil was necessary in order to acquire good detailed flow patterns on the model surface; a trial-and-error procedure was used to determine the proper mix for the particular condition. The oil viscosity was varied over the range from SAE 10-40 weight. Force data were monitored continuously, and the tunnel was run as long as necessary for the measured forces to settle to constant values. The measured force values were not always exactly equal to the values obtained on the clean model but usually were close enough to conclude that the established flow pattern was indicative of the flow taking place about the clean model under the same tunnel conditions.

Sublimation studies were carried out to assess the condition of the boundary layer on the model. These experiments were accomplished by spraying the model with a saturated solution of biphenyl crystals ($C_6H_5C_6H_5$) and petroleum ether. The resulting thin white coating was smoothed by lightly rubbing the surface with a piece of paper. The tunnel then was brought up to test conditions as quickly as possible. As soon as the flow pattern was readily discernible through the viewing port, the tunnel was shut down and the model removed and photographed.

III. Presentation of Results

A. Static Force and Pressure Distribution Results

Figure 3 shows the measured static force acting on the nose at four different pitch angles ($\sigma = 45$, 60, 75, and 90 deg) and a

Table 1 Pressure tap locations: arc length from point 0

Orifice numbers	0	1,25	2,24	3,23	4,22	5,21	6,20	7,19	8,18	9,17	10,16	11,15	12,14	13
Arc length, cm	0	0.95	1.90	2.65	3.40	4.15	4.90	5.85	7.75	8.97	9.71	10.71	11.71	13.61

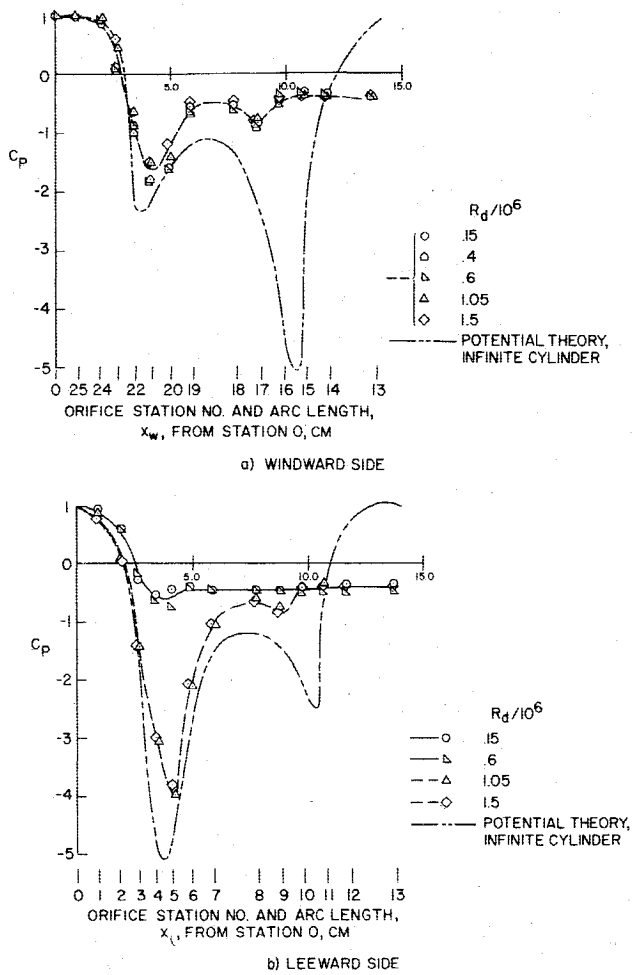

Fig. 4 Pressure distribution at $\sigma = 90$ deg, $\psi = 10$ deg, and $M = 0.25$.

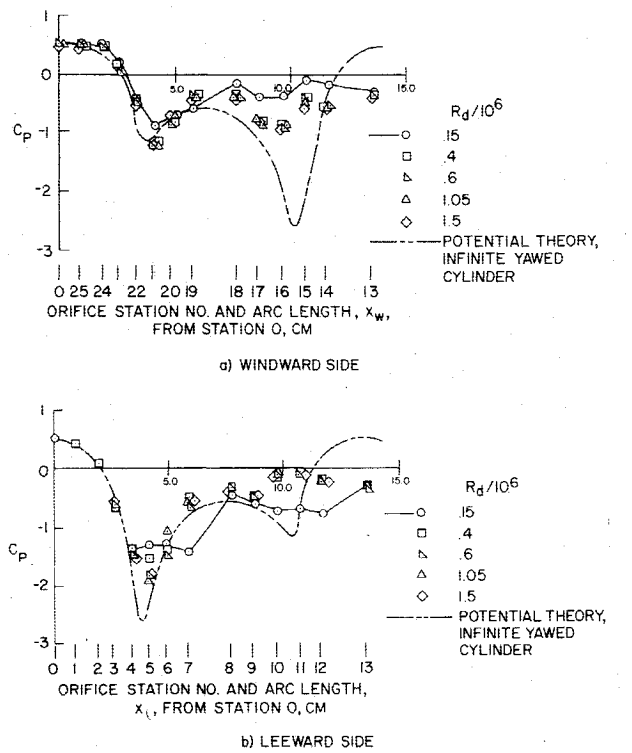

Fig. 5 Pressure distribution at $\sigma = 45$ deg, $\psi = 10$ deg, and $M = 0.25$.

roll angle of $\psi = 10$ deg for a range of Reynolds numbers. Three essential features characterize the data. First, for each σ there is a critical Reynolds number where a drastic change occurs in the side force; second, there is a marked change in the critical Reynolds number with angle of attack; and third, there is a marked change in the character of the side force with angle of attack. The significance of these features will be discussed in Sec. IV.

Figures 4 and 5 show the pressure distributions around the body for angles $\sigma = 90$ and 45 deg, respectively. The windward and leeward distributions (see Fig. 2 for definition of windward and leeward as used in this paper) are given in the (a) and (b) portions of the figures, respectively, for various Reynolds numbers. The abscissas x_w and x_l are measured from station zero, as shown in Fig. 2. Also shown on each figure is the value predicted using the potential theory for an infinite cylinder. This is obtained easily for $\sigma < 90$ deg by multiplying C_p for the $\sigma = 90$ deg case[5] by $\sin^2\sigma$. The agreement between theory and experiment is not particularly good except for a small region on each side of the zero station. The departure from theory is an indication of separation of the boundary-layer flow from the sides of the model.

B. Oil Flow Results

Figures 6 and 7 are photographs of oil flow patterns for $\sigma = 90$ and 45 deg, respectively, for both a high and low Reynolds number. Only the flow patterns observed from the leeward and windward sides are shown. Lines of separation, reattachment, and flow direction are seen readily in these photographs; they will be discussed in detail later.

IV. Analysis and Discussion

The major focus of this section will be to explain the two major features evident in Fig. 3: 1) the occurrence and change with the angle of attack of a critical value of Reynolds number that separates the force behavior into two distinct regions, and 2) the change in character of the forces in these two regions as the angle of attack decreases from 90 to 45 deg. Before considering these two points, it will be instructive to consider the capability of crossflow theory to predict the observed results. One prerequisite that must be met before one even can consider applying crossflow theory to such flows is that the flow over the cylinder be nearly two-dimensional. The evidence for two-dimensionality is discussed below.

A. Two-Dimensionality

Since the research body under discussion has a nearly constant cross section, the flow about the body should be essentially two-dimensional, and the pressure distribution should remain relatively constant with axial station, at least downstream of the hemispherical nose. If this assumption is correct, one should be able to calculate the side-force and normal-force coefficients from the pressure distribution data given in Figs. 4 and 5. The forces obtained from the integrated pressure distributions are compared in Fig. 8. An effective length of 18 cm (7.07 in.) was used for the side-force pressure integrations (which excludes the hemispheric nose, since it has little direct contribution) and 25 cm (9.9 in.) (which includes the effects of the nose) for the normal-force pressure integrations.

The contention that the flow aft of the nose is essentially two-dimensional is supported by this comparison and is substantiated further by the oil flow patterns shown in Figs. 6 and 7 with the notable exception of Fig. 7a, $\sigma = 45$ deg, lee side, which will be discussed in Sec. IVD.

B. Predictions of Crossflow Theory

For inviscid flow, the pressure distribution on an infinite yawed cylinder depends only on the component of flow normal to the body. For example, the forces per unit length (which are proportional to $V_l^2 \sin^2\sigma$) for $\sigma = 45$ deg would be one-half as large as those at $\sigma = 90$ deg for V_l held constant. A simple crossflow theory for the viscous case would suggest that this relation would hold as long as the Reynolds number based on the normal component of flow was the same for the

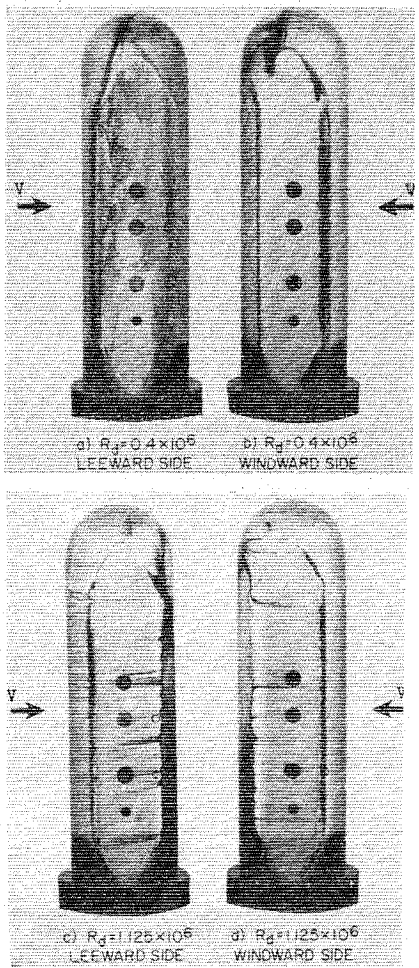

Fig. 6 Oil flow pattern at $\sigma = 90$ deg, $\psi = 10$ deg, and $M = 0.25$.

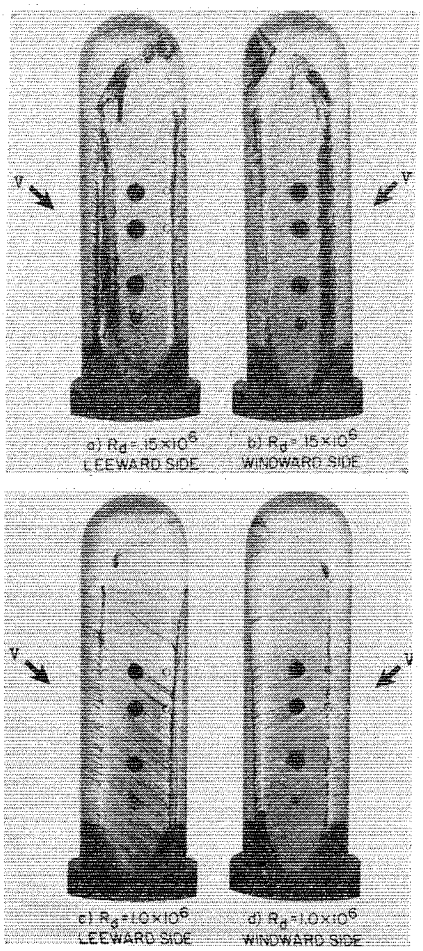

Fig. 7 Oil flow pattern at $\sigma = 45$ deg, $\psi = 10$ deg, and $M = 0.25$.

two different values for σ. Figure 8 shows that this is obviously not true, even though the force data are plotted against R_d instead of R_n. Furthermore, simple crossflow theory would predict that the radical change in side force for $\sigma = 75$ deg should occur at a higher R_d than for $\sigma = 90$ deg. Figure 3 shows that just the opposite happens. Additional insight also can be obtained by comparing pressure coefficients at $\sigma = 90$ deg with those at $\sigma = 45$ deg divided by 0.5, i.e., $\sin^2 45$ deg. This comparison is shown in Fig. 9, where C_{p_n} is plotted vs distance from station 0. The agreement is very good ahead of the separation point; the separation point is at or downstream of the corner for all Reynolds numbers except the lowest one, where it is forward of the corner. Downstream of the separation region, the data do not collapse to a single line; hence, again, the simple crossflow theory should not be expected to provide correct answers.

C. Critical Reynolds Number

As noted earlier, concerning Figs. 3 and 8, there are critical values of Reynolds number at which marked changes in the side and normal forces occur. Some insight into the occurrence of a critical Reynolds number for the normal-force data at $\sigma = 90$ deg can be gained from the analogous but less dramatic change in drag coefficient with Reynolds number which is observed on a circular cylinder normal to the flow.

At low Reynolds number, the boundary layer is laminar and separates readily as it goes around either a circular cylinder or the present shape; the result is a large separated region of flow on the sides and rear of the body. Generally, as the Reynolds number is increased, the boundary layer becomes turbulent ahead of separation, or in some cases the laminar boundary layer can separate and then immediately undergo transition and reattach. Because the flow remains

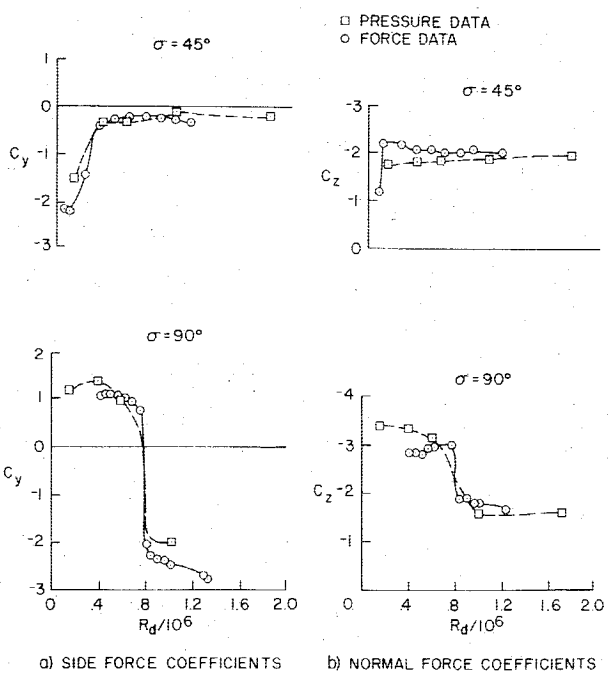

Fig. 8 Comparison of side-force and normal-force coefficients at $M = 0.25$ and $\psi = 10$ deg; from integrated pressure data and static force measurements.

attached further around the body, there is a smaller separated region and hence lower drag for the circular cylinder; and by analogy there is a lower normal force for the present body. A critical Reynolds number also exists for side forces, and its occurrence is discussed later.

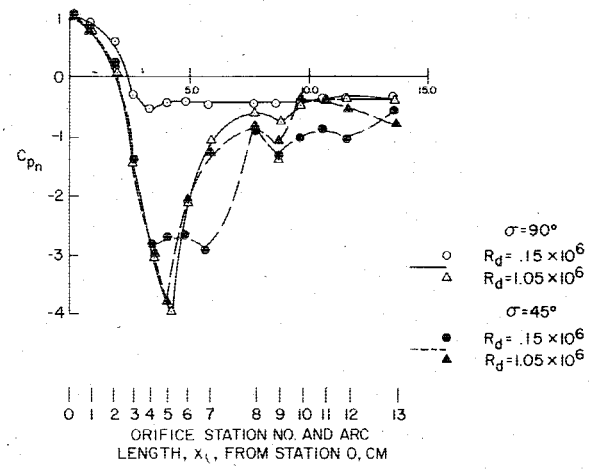

Fig. 9 Comparison between leeside pressure coefficients based on flow component normal to the body axis at $\sigma = 45$ and 90 deg, $\psi = 10$ deg, and $M = 0.25$.

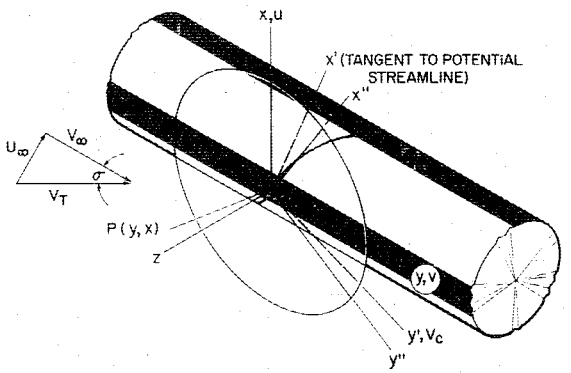

Fig. 10 Definition of axes and velocity components for an infinite yawed cylinder.

In simple crossflow theory, the critical freestream Reynolds number should increase as the angle of attack decreases. This also should be the case for the data for swept circular cylinders of Ref. 6, but in fact the opposite occurs. This failure of simple crossflow theory appears to be a result of a change in the mechanism for transition in the boundary layer from laminar to turbulent flow. It is believed that transition is affected by the three-dimensional nature of the flow and, in particular, by the occurrence of points of inflexion in the boundary-layer profiles, as discussed below.

The term "inflexional instability" arises from hydrodynamic stability theory, where it can be shown that a necessary condition for growth of disturbances propagating in a given direction is that the velocity profile in that direction has a point of inflexion. Furthermore, for the disturbance to be stationary in that direction, the point of inflexion must occur at a point of zero velocity. (For a review of hydrodynamic stability, see Chap. IX of Ref. 7.) As can be seen in Figs. 10 and 11, this is, in fact, the type of profile that exists in most three-dimensional boundary layers. If some point along an infinite yawed cylinder within the laminar boundary-layer region is selected, there will exist a plane containing a normal to the surface at that point such that the boundary-layer velocity vectors projected onto that plane will yield a profile with a point of inflexion occurring at zero velocity.

Referring to Figs. 10 and 11, x is the arc length measured along the surface from the flow dividing line, y is measured parallel to the axis of the cylinder, and z is measured normal to the surface of the cylinder. The corresponding components of the freestream velocity vector in this system of coordinates are u, v, and w. The boundary-layer velocity profiles in this reference system are given in Figs. 11a and 11b. The $y' - x'$

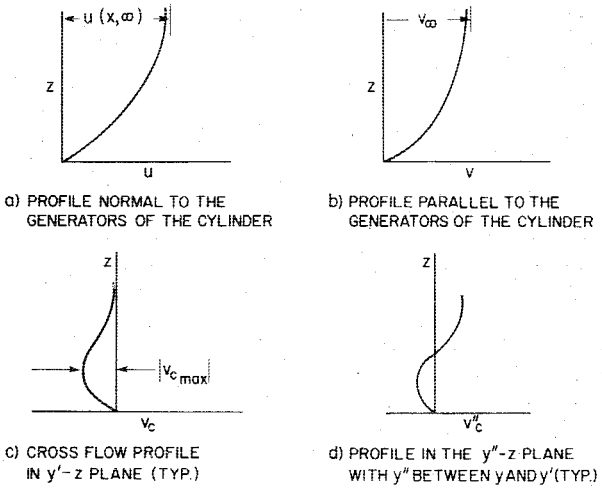

Fig. 11 Sketch of various boundary-layer velocity profiles.

coordinate system depends on x and is chosen so that the x' axis is tangent to the potential streamline at the point $P(y,x)$. This leads to the crossflow velocity profile V_c shown in Fig. 11c, where by definition the velocity vanishes at the wall and at the edge of the boundary layer. Figure 11d represents a profile with the point of inflexion at zero velocity obtained by choosing a set of axes $y'' - x''$ lying in the same plane and originating at the same point as the $y - x$ axes and the $y' - x'$ axes.

When such profiles exist, the boundary-layer flow may exhibit streamwise vortices prior to transition. These vortices were studied by Gregory et al.,[8] who observed them on a spinning disk using a china clay technique. Prior to the preceding work, Owen et al.[9] studied transition from laminar to turbulent flow on swept wings and introduced the concept of a crossflow Reynolds number for correlating transition. Later, Boltz et al.[10] conducted sublimation experiments on an untapered swept wing in the Ames 12-Ft Pressure Wind Tunnel and found good correlation of the appearance of striations (indicating streamwise vortices in the boundary layer) with the crossflow Reynolds number. Chapman[11] showed that the crossflow Reynolds number concept also was useful at supersonic speeds. The effect also has been observed at hypersonic speeds,[12] and calculations of crossflow Reynolds numbers on cones at hypersonic speeds have been carried out by Adams[13] based on numerical solutions of the three-dimensional laminar boundary-layer equations. Additions to the theory on inflexional instability have been published recently, for example, by Tobak.[14]

To check for the existence of these vortices and, hence, the possible reason for the behavior of critical Reynolds number, sublimation tests were run at atmospheric pressure at $M = 0.25$ where $R_d = 0.4 \times 10^6$. These tests were conducted at $\sigma = 45$ and 90 deg, both at $\psi = 10$ deg. For $\sigma = 90$ deg, the flow pattern showed laminar separation on the leeward side with no reattachment, and a laminar separation on the windward side followed by turbulent reattachment. No striations were observed. However, at $\sigma = 45$ deg striations in the biphenyl coating were observed starting at about station 2 on the leeward side (as shown in Fig. 12) and station 23 on the windward side. These striations apparently were due to the small vortices that formed in the boundary layer, with axes roughly aligned with the local flow direction.

Based on the past good correlation of the appearance of striations at a critical crossflow Reynolds number and the subsequent transition to turbulent flow,[9-13] an attempt was made to predict the maximum crossflow Reynolds number for the present case as well as for the cylinder data of Ref. 6. The earlier discussion indicating the high degree of two-dimensionality of the flow suggests treating the portion of the present body, somewhat aft of the herispheric nose, as an

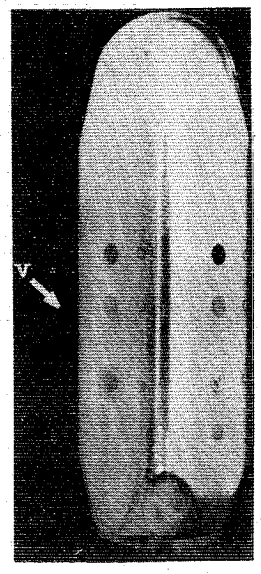

Fig. 12 Sublimation flow pattern on leeside at $R_d = 0.4 \times 10^6$, $\sigma = 45$ deg, $\psi = 10$ deg, and $M = 0.25$.

infinite yawed cylinder, at least upstream of the regions of separated flow. The laminar boundary-layer equations for the infinite yawed cylinder were solved first by Sears[15] for cylinders having a velocity distribution outside the boundary layer of the form

$$u = a_1 x + a_3 x^3 \tag{1}$$

where a_1 and a_3 are constants. Since the striations first appear well ahead of the separated region, it was found that reasonable fits of the form of Eq. (1) could be made to the velocities deduced from the pressure distribution data in Figs. 4 and 5 except near the separated regions. Since striations also were observed on the circular centerbody section behind the model nose, the crossflow Reynolds numbers were calculated for this case as well. A cubic also was found to fit quite well the $\sigma = 45$ deg data of Bursnall et al.,[6] at least up to the separation line. For the boundary-layer calculations in the x direction, the tables of Tifford[16] were used, and for the y direction the tables of Goertler appearing in Schlichting[17] were used. A portion of Tifford's tables also appear in Ref. 17, together with an account of Sears' method of solution. The w component of velocity was neglected.

Equation (1) implies, of course, that the cylinder cross section is symmetric about an axis through the stagnation point. The use of the cubic for the nonsymmetric case was believed to be justified by the fact that the pressure distribution on each side of the present body near the flow dividing line was approximately the same. (The flow dividing line corresponds to the stagnation line for the normal component of velocity. Strictly speaking, the flow dividing line is not a stagnation line.) The $u(x,z)$ and $v(x,z)$ velocity profiles were calculated at discrete values of x for $\sigma = 45$, 60, and 75 deg, both for the present body and for a circular cylinder (diameter = 7.62 cm), over a range of Reynolds numbers. The maximum crossflow velocity for each x was determined by projecting the u and v components onto the $y' - z$ plane defined in Fig. 10. At each x, the displacement thickness δ^*, based on $u(x,z)$, was calculated, and a crossflow Reynolds number then was calculated at each x from

$$R_c = 3\delta^* |V_c|_{\max} / \nu \tag{2}$$

where $3\delta^*$ is approximately equal to that value of z where the velocity in the boundary layer equals 99% of the potential flow velocity. The $3\delta^*$ was used instead of δ^* to make the definition of R_c comparable to that used in Refs. 8-10. For the present body, the maximum R_c occurred between stations 2 and 3 on the leeward side (Fig. 2).

For the method of calculation used, it can be shown that R_c is directly proportional to $\sqrt{R_d}$. However, for convenience the maximum values of R_c for the various conditions calculated are summarized in Table 2. The conditions for which sublimation tests were made are indicated. It is immediately obvious that more experimental evidence is needed to define the lower limits for the appearance of striations. For several reasons, however, it is believed that $R_d = 0.4 \times 10^6$, where the striations were observed, is near the lower limit. First, $R_c = 119$ for the circular cylinder compares with the lower limit of about 125 from Refs. 10 and 11 for swept wings. Second, the critical Reynolds number for drag increase for a 45-deg swept circular cylinder is about 0.4×10^6 (Ref. 6). A brief set of calculations was made for a circular cylinder at $\sigma = 30$ deg and, when compared with the data of Ref. 6, yielded $R_c = 105$. Figure 3 shows a change in behavior of C_y at $\sigma = 45$ deg and $R_d = 0.4 \times 10^6$ which would indicate that the value of $R_c = 89$ for the present body would represent the lower limit for striations to appear (see Table 2). There is some additional evidence[6] that $R_c = 125$ is not a universally applicable number for the lower limit. For the present body, if the lower limit of R_c is taken to be between 85 and 90, one would expect to see a change in behavior of the side force at $\sigma = 60$ deg between $R_d = 0.6 \times 10^6$ and 0.7×10^6. Referring to Fig. 3 for $\sigma = 60$ deg, it can be seen that such a change does take place. By referring to the C_y curves on Fig. 3, it can be

Table 2 Maximum crossflow Reynolds number as a function of R_d

	$\sigma = 45$ deg			$\sigma = 60$ deg			$\sigma = 75$ deg		
R_d	Circular	Square body		Circular	Square body		Circular	Square body	
10^6	cylinder	Leeward	Windard	cylinder	Leeward	Windard	cylinder	Leeward	Windard
0.1	60	44	49	43	35	36	22	23	19
0.2	84	63	70	60	49	51	31	32	28
0.3	103	77	85	74	61	62	38	39	34
0.4[a]	119[a]	89[a]	99[a]	85	70	73	44	45	39
0.5	134	99	110	95	78	80	49	50	44
0.6	146	108	121	105	86	88	54	55	48
0.7	158	117	131	113	93	95	58	60	52
0.8	169	125	140	121	99	102	62	64	55
0.9	179	133	148	128	105	108	66	68	58
1.0	189	140	156	135	111	114	70	71	62
1.1	198	147	164	142	116	119	73	75	65
1.2	207	153	171	148	121	124	76	78	67
1.3	215	160	178	154	126	129	79	81	70
1.4	223	166	185	160	131	134	82	84	73
1.5	231	171	191	165	136	139	85	87	75

[a] Striations observed in sublimation test.

seen that the critical value of R_d for $\sigma = 90$ deg is about 0.8×10^6 and about 0.7×10^6 for a $\sigma = 75$ deg, which is a change in the expected direction. However, the calculations show that R_c does not reach the critical value for $\sigma = 75$ deg until about $R_d = 1.5 \times 10^6$, which is well past the critical Reynolds number of 0.8×10^6 for the $\sigma = 90$-deg case. It is possible, however, for the inflexional nature of the profiles to trigger earlier transition without the appearance of striations.

Another assessment of the boundary-layer calculations just described can be made by using them to find the $y'' - x''$ axes at the points where the striations first appear in Fig. 12. These calculations give an angle of 54 deg between the striations and the y axis. The measured value of this angle is about 55 deg.

The foregoing analysis strongly supports the idea that the critical Reynolds number at which changes in aerodynamic forces occur depends on the nature of the boundary layer and the associated effects on separation. Furthermore, the change in critical Reynolds number with angle is due to the laminar boundary-layer profiles with points of inflexion that promote transition from laminar flow to turbulent flow at lower Reynolds numbers than is the case for $\sigma = 90$ deg. The analysis indicates that the inflexional profiles result in the appearance of small streamwise vortices in the boundary layer for $\sigma \leq 60$ deg which can be correlated with a critical crossflow Reynolds number R_c of about 80 to 90.

D. Change in Character of Forces with Angle of Attack

The last major point of the analysis is the change in character of the force with angle of attack. As discussed earlier, simple crossflow theory failed to explain the behavior of the critical Reynolds number. The normal-force characteristics at $\sigma = 90$ deg are understood easily by comparison to the drag coefficient behavior and separation on a circular cylinder, as described earlier. The anomalous behavior of the side force can be explained in terms of the same separation pattern, as was described in Ref. 5; it is discussed below. First, however, the separated flow model on the body that is believed to account for the observed forces will be stated, and then the evidence for it will be considered in detail.

First, the separated flow model associated with the $\sigma = 90$ deg case that was studied thoroughly by Polhamus[5] will be discussed. Above the critical Reynolds numbers, the flow remains attached around the two front corners, or separates and immediately reattaches, with the boundary layer remaining either attached or very close to the sides of the body as it passes downstream into a relatively small wake. Below the critical Reynolds numbers, the flow separates at or forward of the front corners with the separated boundary layer far removed from the body, particularly on the leeward side. The second feature of the flow model is that, as the angle of attack is decreased from $\sigma = 90$ deg, axial flow or the vortices originating at the nose apparently organize the normally highly disorganized wake that occurs near $\sigma = 90$ deg. This organization effectively vents the separated region and causes a favorable pressure gradient, which delays separation and results in a smaller wake and a larger region of attached flow.

To understand the application of this separation model to this geometry and the effect on the resulting forces, separation needs to be considered in the light of the deviation from the pressure distributions calculated from potential flow theory shown in Figs. 4 and 5. A large negative peak occurs on the first leeward and second windward corners, and a smaller negative peak occurs on the other two corners. Since the flow is potential, no net forces are produced. The measured forces result from the flow downstream of separation, where the pressures deviate drastically from the potential solution, normally eliminating any further significant low-pressure peaks or full pressure recovery at the rear stagnation line.

When the separation flow model is combined with the pressure distribution for $\sigma = 90$ deg, it is found, as was described in Ref. 5, that above the critical Reynolds number (Figs. 4, 6c, and 6d) the flow remains attached fairly well around the first leeward corner and all of the way around the first windward corner, separating just ahead of both second corners. Very short separation bubbles may exist on the first two corners. The result is that the side force is dominated by the low-pressure peak on the first leeward corner and results in a negative value of side force. The normal force C_z is dominated by the poor pressure recovery on the back but is determined partially by the thrust from the low pressures on the first two corners. Below the critical Reynolds number (see Figs. 4, 6a, and 6b), the flow separates ahead of the first corner on the leeward side, completely eliminating the low-pressure peak. On the windward side, the separation bubble is larger, but the flow downstream has reattached. This results in the side force being dominated by the smaller low-pressure peak on the first windward corner and hence a positive side force C_y opposite to that above the critical Reynolds number. The normal force C_z is increased greatly because of the loss of thrust on the first leeward corner.

Now consider the same model at $\sigma = 45$ deg, with the additional proposition that the axial flow and the wake vortices from the nose (stable vortices starting in the nose region were observed in water-tunnel tests on this body conducted at the University of Florida) have partially vented the separation region, and the resulting favorable pressure gradient provides more attached flow. First, the potential flow pressures are half as large as they are at $\sigma = 90$ deg; hence, one would expect the forces to be significantly less. Above the supercritical Reynolds numbers, this is indeed the case for the side force (refer to Fig. 8), but it is even smaller than a factor of 2, suggesting that the flow may be attached farther around the body, resulting in additional cancellation of the pressure forces from the two sides of the body. This can be seen by comparing the oil flow pictures from Figs. 6c and 6d with Figs. 7c and 7d. The normal force has increased slightly, rather than decreased by a factor of 2. The reason for this is not understood entirely but is probably a result of the axial flow (vortices) yielding a lower pressure (vortex lift) on the back side of the body and, hence, a higher normal force. Below the critical Reynolds number, the venting caused by the axial flow and vortex flow has an even larger effect (Figs. 7a and 7b). The flow now remains attached around the first two corners, particularly the leeward corner, yielding again a large negative side force.

V. Conclusions

The behavior, at high angles of attack, of the change with Reynolds numbers in force characteristics on a research body has been studied in detail. In general, the force characteristics are shown to be mainly a function of when separation occurs and whether reattachment takes place on the leeward side of the body. Both specific and general conclusions are drawn from the results of the present test; some specific conclusions are discussed below:

1) For each angle of attack there is a critical Reynolds number wherein large changes in the forces are observed. These changes are primarily a function of the separation pattern on the body and are closely coupled with transition from laminar to turbulent flow.

2) As the angle of attack decreases, the critical Reynolds number based on freestream conditions decreases from 0.8×10^6 at $\sigma = 90$ deg to 0.4×10^6 at $\sigma = 45$ deg. Predictions based on crossflow theory indicate that the critical freestream Reynolds number should increase with decreasing angle of attack. It is shown convincingly in this paper that the process controlling transition gradually changes from the process at $\sigma = 90$ deg to a process resulting from inflexional instabilities in the boundary layer for σ between 60 and 75 deg.

3) As the angle of attack decreases from 90 deg, the variation of forces, and particularly the side force, with Reynolds number reverses. There is strong evidence that this

reversal is due to vortices forming in the wake at $\sigma < 90$ deg. These vortices apparently vent the separated region, contributing to the formation of a more favorable pressure gradient than at $\sigma = 90$ deg; hence they delay separation or encourage reattachment. Delaying separation on the leeward side accounts for the reversal of the side forces.

Although the results discussed herein are for a research body, the insight into high-angle-of-attack flowfields which has been gained can be applied to other bodies and may be useful in explaining the contributions of the aircraft forebody to spin aerodynamics. Although not discussed directly in this paper, the results of the static tests described herein and the spin tests of Ref. 3 are very similar. Therefore, based on the success in predicting the detailed features of the static flow about this research body, it is believed that the general features of spin aerodynamics due to contributions from aircraft fuselages of similar cross-sectional shapes can be predicted.

Acknowledgments

The authors would like to thank Earl Keener of Ames Research Center for his help on the oil flow and sublimation studies, William Hyatt, a graduate student at the University of Florida, for performing the boundary-layer calculations, and Morrow Whitcomb, Project Engineer of ARO, Inc., for overseeing the operational aspects of conducting the test in the wind tunnel.

References

[1] Clarkson, M. H., Malcolm, G. N., and Chapman, G. T., "Experimental Post-Stall Rotary Aerodynamic Coefficients for Airplane-Like Configurations," *Journal of Aircraft*, Vol. 13, Aug. 1976, pp. 565-570.

[2] Allen, H. J. and Perkins, E. W., "A Study of the Effects of Viscosity on Flow Over Slender Inclined Bodies of Revolution," NACA TR 1048, 1951.

[3] Malcolm, G. N. and Clarkson, M. H., "Wind Tunnel Testing with a Rotary-Balance Apparatus to Simulate Aircraft Spin Motions," *AIAA 9th Aerodynamic Testing Conference*, Arlington, Texas, June 1976, pp. 143-156.

[4] Polhamus, E. C., "Effect of Flow Incidence and Reynolds Number on Low-Speed Aerodyanmic Characteristics of Several Noncircular Cylinders with Applications to Directional Stability and Spinning," NACA TN 4176, 1958.

[5] Polhamus, E. C., Geller, E. W., and Grunwald, K. H., "Pressure and Force Characteristics of Noncircular Cylinders as Affected by Reynolds Number with a Method Included for Determining the Potential Flow about Arbitrary Shapes," NASA TR R46, 1959.

[6] Bursnall, W. J. and Loftin, L. K., Jr., "Experimental Investigation of the Pressure Distribution about a Yawed Circular Cylinder in the Critical Reynolds Number Range," NACA TN 2463, 1951.

[7] Rosenhead, L. (ed.), *Laminar Boundary Layers*, Oxford Press, London, 1963.

[8] Gregory, N., Stuart, J. T., and Walker, W. E., "On the Stability of Three-Dimensional Boundary Layers with Applications to the Flow Due to a Rotating Disk," *Philosophical Transactions of the Royal Society of London*, Ser. A, Vol. 248, No. 943, July 1955, pp. 155-199.

[9] Owen, P. R. and Randall, D. G., "Boundary Layer Transition on a Swept Back Wing," Royal Aircraft Establishment, TM Aero. 277, May 1952.

[10] Boltz, F. W., Kenyon, G. C., and Allen, C. Q., "Effects of Sweep Angle on the Boundary-Layer Stability Characteristics of an Untapered Wing at Low Speeds," NASA TN D-338, 1960.

[11] Chapman, G. T., "Some Effects of Leading-Edge Sweep on Boundary-Layer Transition at Supersonic Speeds," NASA TN D-1075, 1961.

[12] McDevitt, J. B. and Mellenthin, J. A., "Upwash Patterns on Ablating and Nonablating Cones at Hypersonic Speeds," NASA TN D-5346, 1969.

[13] Adams, J. C., Jr., "Three-Dimensional Boundary Layer Analysis of Upwash Patterns and Entrained Vortex Formation on Sharp Cones at Angles of Attack," Arnold Engineering Development Center, AEDC-TR-71-215, Dec. 1971.

[14] Tobak, M., "On Local Inflexional Instability in Boundary Layer Flows," *Zeitschrift fur angewandte Mathematik und Physik*, Vol. 24, Fasc. 3, 1973, pp. 330-354.

[15] Sears, W. R., "The Boundary Layer of Yawed Cylinders," *Journal of the Aeronautical Sciences*, Vol. 15, Jan. 1948, pp. 49-52.

[16] Tifford, A. N., "Heat Transfer and Frictional Effects in Laminar Boundary Layers, Part 4," Wright Air Development Center, TR 53-288, Aug. 1954.

[17] Schlichting, H., *Boundary-Layer Theory*, McGraw-Hill, New York, 6th ed.